

Statistical hadronization of heavy quarks in ultra-relativistic nucleus-nucleus collisions

A. Andronic^a, P. Braun-Munzinger^{a,b}, K. Redlich^c, J. Stachel^d

^a*Gesellschaft für Schwerionenforschung, GSI, D-64291 Darmstadt, Germany*

^b*Technical University Darmstadt, D-64289 Darmstadt, Germany*

^c*Institute of Theoretical Physics, University of Wrocław, PL-50204 Wrocław, Poland*

^d*Physikalisches Institut der Universität Heidelberg, D-69120 Heidelberg, Germany*

Abstract

We present new results on the statistical hadronization of heavy quarks at SPS, RHIC and LHC energies. Several new aspects are considered, among them a separation of the collision geometry into a “core” and a “corona” part and an estimate of the annihilation rate of charm quark in a hot plasma, together with a critical assessment of its influence on the results. For RHIC energies we investigate the centrality dependence of J/ψ production focusing on the model results for different values of the charm production cross section, including its theoretical and experimental uncertainty. We also study, within this model, the rapidity dependence of the J/ψ yield. Recent RHIC data from the PHENIX experiment are well reproduced. At LHC energy, we update our model predictions for the centrality dependence of the J/ψ yield and investigate as well the rapidity dependence. We also discuss the transverse momentum distributions of J/ψ mesons expected from the model and provide predictions for a range of values of the expansion velocity at chemical freeze-out. Finally, we extend the model to predict Υ yields in Pb+Pb collisions at LHC energy.

1 Introduction

The idea of statistical hadronization of charm quarks in nucleus-nucleus collisions [1] has led to a series of investigations of J/ψ production based on this approach [2,3,4,5,6]. Initial interest focussed on the available SPS data for J/ψ production in Pb-Pb collisions, but the trends for RHIC and LHC were also investigated. An independent approach, based on a kinetic model [7,8,9] has been developed in parallel. Recently the statistical hadronization model was extended to the production of Υ mesons [10] and multiply heavy-flavored hadrons [11].

We have shown earlier [1,5] that the J/ψ data at SPS energy can be described within the statistical approach, but only when assuming that the charm production cross section is

enhanced by about a factor of 3 beyond the perturbative QCD (pQCD) predictions. For RHIC energy, the predictions of our model were shown [5] to be in good agreement with the early PHENIX J/ψ data [12] as well as with the relative yields of open charm mesons measured by STAR [13].

We focus in this paper on the production of charmonia in nucleus-nucleus collisions at RHIC (Au-Au, $\sqrt{s_{NN}}=200$ GeV) and LHC (Pb-Pb, $\sqrt{s_{NN}}=5.5$ TeV) energies within the framework of the statistical hadronization model, SHM [1,5]. Particular emphasis is placed on the rapidity and transverse momentum dependence of J/ψ and, for LHC energy, also Υ production. Section 2 contains a brief summary of the main ingredients of the model along with a description of recent updates concerning the chemical freeze-out parameters, the spectrum of open charm mesons and baryons, and the values of charm production cross section. Furthermore, for a more realistic description of the centrality dependence in nucleus-nucleus collisions, we separate the collision geometry into a 'core' and a 'corona' part.

In Section 3, we provide an estimate of the magnitude of $c\bar{c}$ annihilation in the expanding quark-gluon plasma (QGP).

In Section 4, we use the model to predict phase space distributions of quarkonia produced in nucleus-nucleus collisions. We compare the results with SPS data and with preliminary data available at RHIC [14] and provide predictions for the LHC energy, where data [15] are expected in about two years. In particular the situation at SPS energy is significantly modified when taking into account the realistic reaction geometry. We extend the model for the calculation of Υ yields in Pb+Pb collisions at LHC energy. In this case, despite the similarity in production rates of bottom at LHC with charm at RHIC [16], the applicability of our model may be questionable, as the thermalization of the bottom quarks may be debatable. We discuss below the main sources of uncertainty in these calculations.

2 The model and its inputs

The statistical hadronization model (SHM) [1,5] assumes that all heavy quarks (charm and bottom) are produced in primary hard collisions and that their total number stays constant until hadronization. The validity of this latter point is investigated in the next section. Another important factor is thermal (but not chemical) equilibration in the QGP, at least near the critical temperature, T_c . The quarkonia are then all produced (non-perturbatively) when T_c is reached and the system hadronizes. Our picture is different from the one of color screening [17] (see [18] for a more recent account), which assumes that formation of quarkonia takes place before a thermalized QGP is established but is suppressed in the QGP when the temperature reaches a certain threshold, which is species dependent. Recent results from solving Quantum Chromodynamics (QCD) on the lattice indicate indeed that J/ψ mesons could survive in the QGP up to $1.6T_c$ [19], implying, e.g. little melting at SPS energies. Further investigations indicate that Υ mesons may survive up to temperatures of at least $2.3T_c$ [20].

In the SHM, we assume that (i) no quarkonia production takes place before the formation time τ_0 of the QGP or (ii) that all quarkonia formed before τ_0 are melted in the initial hot

QGP phase. Under this scenario the possible existence of bound quarkonia states in the QGP is not important, since the estimates made in the next section demonstrate that, unless there is a resonance-like enhancement of the cross section, formation of quarkonia from uncorrelated c and \bar{c} quarks in the expanding plasma is very unlikely even if such states exist as bound states.

Thermal equilibration of charm quarks in a QGP ¹ is currently investigated vigorously both experimentally and theoretically. In particular, elliptic flow of charm quarks [22] has been demonstrated within a coalescence approach [23,24] to be a very sensitive probe of thermalization. Large elliptic flow is obtained in hydrodynamic simulations based on the diffusion coefficient of charm quarks in a QGP [25]. Elliptic flow of J/ψ is smaller in recent hydrodynamic calculations [26] than in coalescence models [27]. Remarkably, the experimental results on the elliptic flow of electrons from charm mesons ("non-photonic" electrons) [28] do indicate that charm quarks indeed thermalize to a significant degree. In addition, a large energy loss of charm quarks in the QGP [29] has been recently found by experiments [30,31]. The experimental results of PHENIX [31] indicate in fact a larger energy loss than theoretically expected [32]. The mechanism for charm thermalization is not well understood. A model based on resonant rescattering of heavy quarks in the QGP [33] reproduces quite well the experimental results. It is worth noticing that in this model the thermalization time for heavy quarks is substantially reduced compared to the case of perturbative interactions [33]. In transport models the measured elliptic flow can be reproduced only for a charm quark scattering cross section that is much larger than the cross sections computed within perturbative QCD [34,35]. In any case, we note that the SHM can be applied even if charm thermalization is reached only close to T_c .

In the following we briefly outline the calculation steps in our model [1,5]. The heavy quark (charm or bottom) balance equation [1], which has to include canonical suppression factors whenever the number of charm or bottom pairs is not much larger than 1, is used to determine a fugacity factor g_c via:

$$N_{c\bar{c}}^{dir} = \frac{1}{2}g_c N_{oc}^{th} \frac{I_1(g_c N_{oc}^{th})}{I_0(g_c N_{oc}^{th})} + g_c^2 N_{c\bar{c}}^{th}. \quad (1)$$

Here $N_{c\bar{c}}^{dir}$ is the number of directly produced $c\bar{c}$ pairs and I_n are modified Bessel functions. In the fireball of volume V the total number of open ($N_{oc}^{th} = n_{oc}^{th}V$) and hidden ($N_{c\bar{c}}^{th} = n_{c\bar{c}}^{th}V$) charm hadrons is computed from their grand-canonical densities n_{oc}^{th} and $n_{c\bar{c}}^{th}$, respectively. The densities of different particle species in the grand canonical ensemble are calculated following the statistical model [36,37,38]. The balance equation (1) defines the fugacity parameter g_c that accounts for deviations of heavy quark multiplicity from the value that is expected in complete chemical equilibrium. Since in the SHM the charm and bottom quark yields are completely determined by their production in initial (hard) collisions the fugacity factor can be very large, especially for bottom production. The yield of charmonia of type j is obtained as: $N_j = g_c^2 N_j^{th}$.

To illustrate some essential features of the model, we show in Fig. 1 the centrality de-

¹ The cross sections for production of charmed quarks are much too small to allow for their chemical equilibration in a QGP at reasonable ($T < 1$ GeV) temperatures, as is demonstrated in [21].

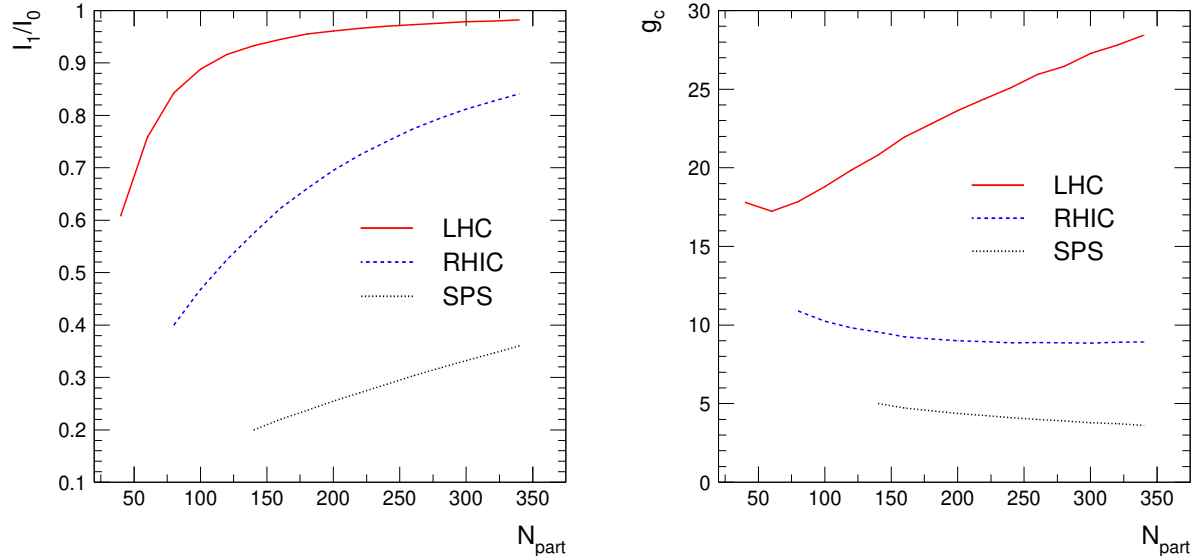


Fig. 1. Centrality dependence of the canonical suppression for charm, I_1/I_0 (left panel) and of the charm quark fugacity, g_c (right panel) for SPS, RHIC and LHC energies.

pendence of the canonical suppression factor, I_1/I_0 , and of the charm quark fugacity, g_c , for SPS, RHIC and LHC energies. The inputs for the calculations are discussed below. It is clear that at SPS and RHIC energies, where the number of $c \bar{c}$ pairs especially for more peripheral collisions is not much larger than 1, the centrality dependence of the J/ψ yield, controlled by the g_c parameter, is determined by the canonical suppression. At LHC energy this is a rather weak effect, owing to a much larger charm production cross section and to a larger volume at freeze-out (hadronization). We note that an important check of the validity of the statistical hadronization model is the $\psi'/J/\psi$ yield ratio. The model predictions agree with the earlier data at the SPS energy [1] and we will discuss the present status in Section 4. The model has the following physical input parameters: i) the temperature, T , and baryochemical potential, μ_b , for statistical model calculations; ii) the heavy quark production cross section in nucleon-nucleon interactions; iii) the volume of one unit of rapidity, $V_{\Delta y=1}$ at chemical freeze-out. We discuss them below, with special emphasis on the updates used here relative to our previous set of predictions [5].

Based on our recent analysis of hadron yields within the thermal model [38], we use here (T, μ_b) of (161, 22.4) MeV for RHIC and (161, 0.8) MeV for LHC. The uncertainty in T is 4 MeV and we have shown previously [5] that the outcome of SHM results exhibit little sensitivity to the precise value of T . Note that the thermal parameters have been determined from fits of data at midrapidity in central collisions. From the measured particle abundancies [39], the centrality dependence of T and μ_b at RHIC is expected to be weak. Based on the measured rapidity dependence of particle ratios at RHIC [42] it is expected that (T, μ_b) will be different away from midrapidity (in particular, μ_b is expected to increase), but this has a rather small influence on the model results in the present context.

In order to have accurate calculations, it is important to include the complete spectrum of open charm states. Based on the latest updates of the Particle Data Group [40], compared to our previous results [5], we have added for the present calculations 10 new charmed mesons ($D_0^*(2400)$, $D_1(2420)^\pm$, $D_{s0}^*(2317)$, $D_{s1}(2460)$) and 12 new charmed

baryons ($\Sigma_c(2520)$, $\Xi_c^0(2646)$, $\Xi_c'^{+,0}$) plus their anti-particles. We now have in the code (including antiparticles) 40 charmed meson states and 32 charmed baryon states. As a consequence of these updates, the J/ψ yield is reduced by 12% at RHIC and by 16% at LHC energy as compared to the results obtained with the previous, less complete, spectrum. Even if the spectrum of charmed hadrons may still not be complete at this stage, the effect of further missing states on the J/ψ yield is suppressed because of their mass.

To get a feeling for the size of the effect we have investigated the following scenario: some of the above new meson resonances are interpreted [41] as chiral partners of the known charmed hadrons. Within this approach, their mass is about 300 to 400 MeV larger than for the "ordinary" charmed hadrons. It is easy to estimate that, in a thermal approach, the abundancy of all possible still missing charm states is about 10% of the abundancy of "ordinary" charmed hadrons, which would be equivalent to a reduction of the charm production cross section in proportion. As we discuss below, the uncertainty in the charm production cross section is much larger and dominates the uncertainty of our model predictions.

The spectrum of open bottom mesons and baryons is poorly known in comparison to the charm sector. To partially overcome this difficulty, we have added, besides the known states [40], excited states with masses derived via an analogy with the charm mesons and baryons. Despite this, we should clearly state that our predictions on Υ production, which we pursue here for the LHC energy, are an upper bound.

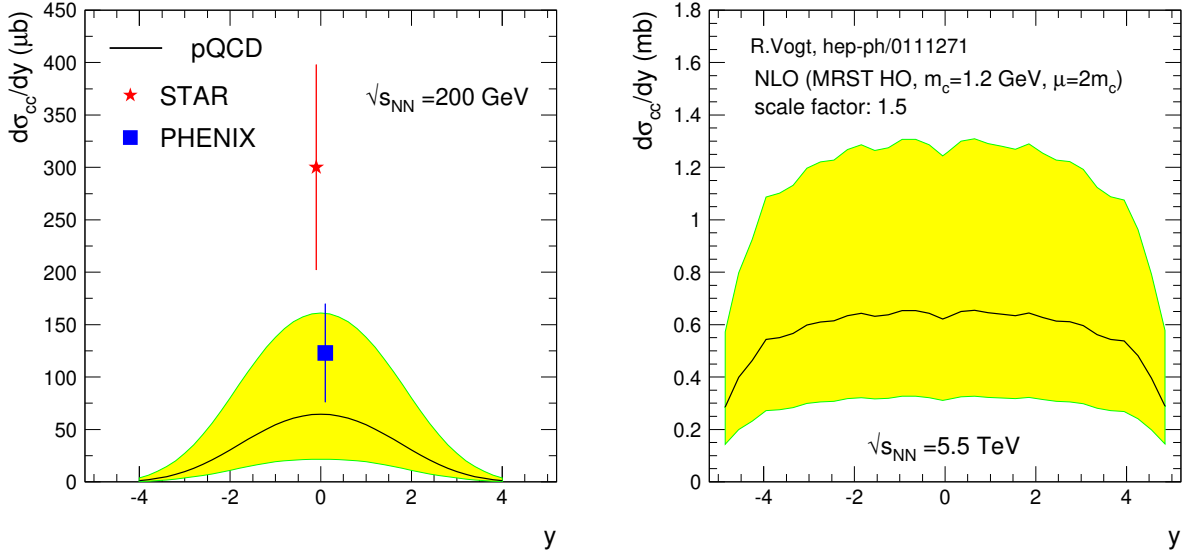


Fig. 2. Rapidity dependence of the charm production cross section in pp collisions. Left panel: for RHIC energy, pQCD calculations [44] and experimental values [48,49]. Right panel: for LHC energy, NLO calculations of ref. [43] scaled up by a factor of 1.5.

The charm production cross section in nucleon-nucleon interactions is, in absence of direct measurements, taken from perturbative QCD (pQCD) calculations. For SPS energy we use the rapidity density of the charm cross section of ref. [43]. For the RHIC energy, we have adopted the recent pQCD calculations [44], which include a careful estimate of the theoretical systematic errors. It was shown earlier [43] that, at RHIC energy, shadowing of the parton distribution functions (PDF) in AA collisions is a minor effect. For LHC energy

we have adopted the NLO calculations of ref. [43], where shadowing for AA collisions is included. In these calculations the intrinsic k_T broadening of partons ($\langle k_T^2 \rangle = 1 \text{ GeV}^2$) is supplemented by a nuclear broadening of 0.7 GeV^2 ($A=200$). Further, we have scaled up these pQCD calculations by a factor of 1.5 to bring them in agreement with more recent results [45] (see discussion in [46]). Following the study made in [44] we have assumed the systematic errors of the cross section to be a factor 2 for SPS and LHC energy. From the cross section, we calculate the number of produced $c\bar{c}$ pairs as: $N_{c\bar{c}} = \sigma_{c\bar{c}} \cdot T_{AA}$, where T_{AA} is the nuclear overlap function, calculated using [47].

The rapidity distributions of the charm production cross section in pp collisions for RHIC and LHC energies are shown in Fig. 2. As seen in the left panel in Fig. 2, at RHIC the extracted experimental charm production cross section at midrapidity of PHENIX [49] of $123 \pm 47 \mu\text{b}$ is, within the errors, in agreement with the pQCD calculations of $d\sigma_{c\bar{c}}^{pQCD}/dy = 63.7_{-42.3}^{+95.6} \mu\text{b}$ [44]. The measured value of $300 \pm 98 \mu\text{b}$ by STAR [48] is significantly larger. Note that the experimental values are extracted mostly from single electron spectra [48,49], a difficult measurement which is reflected in the size of the errors. It was shown [44] that the PHENIX single electron transverse momentum (p_t) spectra [50] are compatible with the upper limit of the systematic errors for the pQCD calculations, as also seen in Fig. 2 for the p_t -integrated value. We note that, at Tevatron, the measured cross section of D mesons [51] was underpredicted by pQCD calculations [52] by up to a factor of 2 for the lowest measured transverse momentum ($\simeq 5 \text{ GeV}/c$). However, in more recent calculations [53] this discrepancy is reduced to a factor of 1.5, so that now data and theory are compatible within errors.

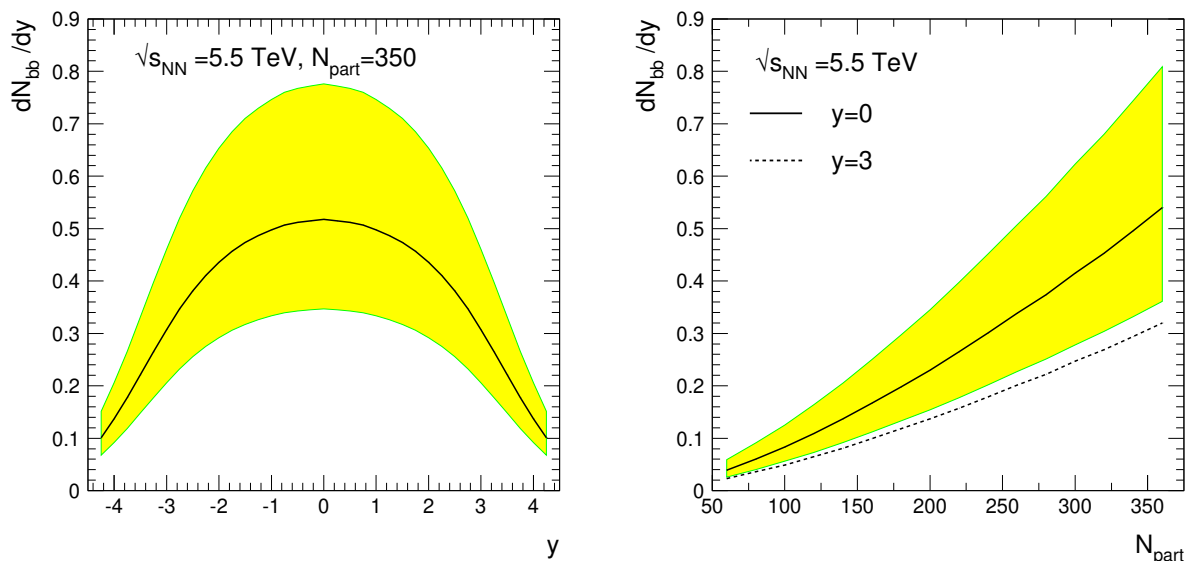


Fig. 3. Rapidity (left panel, for central collisions) and centrality dependence (right panel) of the number of $b\bar{b}$ pairs per unit of rapidity. The lines are for the central value of the bottom cross section [43], the shaded areas are bounds for the uncertainty.

For bottom production cross sections we use the pQCD calculations of ref. [43]. For the uncertainty of the cross section we assume a factor of 1.5 up and down. In Fig. 3 we show the bottom quark pair production rates as a function of rapidity for central Pb-Pb collisions and as a function of centrality for $y=0$ and $y=3$.

In our approach all charmonia are formed by $c\bar{c}$ recombination at the phase transition. An interesting question is the volume within which recombination can take place. A natural size for this quantity is the volume corresponding to a slice of one unit of rapidity. We have shown earlier [5] that, at RHIC, the dependence of the results on the magnitude of the rapidity width is small, as long as intervals of 1-3 units of rapidity are considered. This dependence is even smaller for the LHC case. The volume $V_{\Delta y=1}$ is obtained from the calculated thermal densities and the experimental values of charged particles rapidity densities, dN_{ch}/dy , at midrapidity. For central collisions (number of participating nucleons $N_{part}=350$) we obtain at SPS $V_{\Delta y=1}=1200 \text{ fm}^3$, while at RHIC, $dN_{ch}/dy=701$ leads to $V_{\Delta y=1}=2400 \text{ fm}^3$ [38]. At LHC, based on a recently-proposed parametrization [54] of the energy dependence of dN_{ch}/dy , the expected value is $dN_{ch}/dy=1816$, leading to $V_{\Delta y=1}=6200 \text{ fm}^3$ at midrapidity. This presently used value of dN_{ch}/dy at LHC is slightly lower than our previous phenomenological extrapolation [5]. We have shown earlier [5] that the uncertainty in the volume is affecting the model predictions rather marginally. Our previous results [5] were obtained assuming a linear scaling of dN_{ch}/dy (and consequently $V_{\Delta y=1}$) with N_{part} . For the present calculations the scaling is done for the 'core' region only (see below).

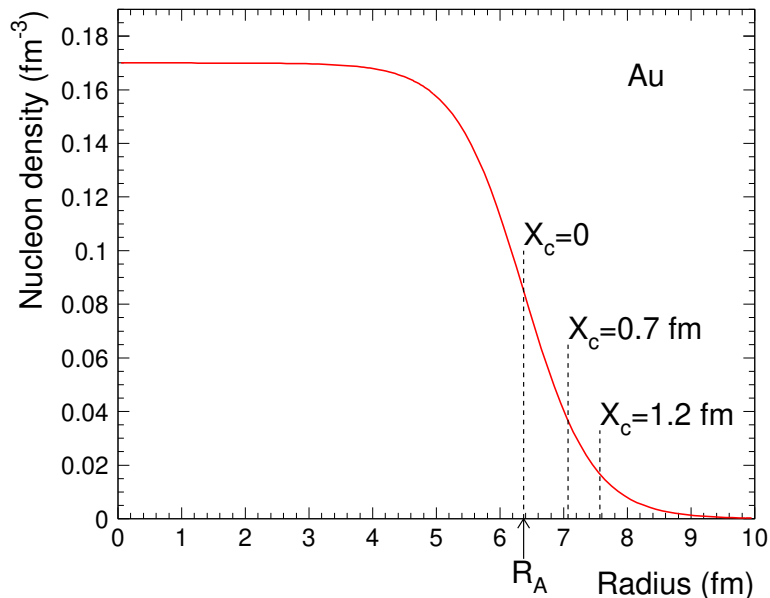


Fig. 4. The nuclear density (Woods-Saxon) distribution for the Au nucleus. The core corresponds to the radius $R_A + X_c$, beyond this radius the nucleons are in the corona region.

An important effect to be included when studying centrality dependence in nucleus-nucleus collisions is the so-called "corona effect", a fact which has been emphasized recently [55]. In the present approach the number of participating nucleons, N_{part} , as well as the number of binary collisions, N_{coll} , are calculated assuming Woods-Saxon nuclear density distribution. However, it is appropriate to distinguish the nucleons close to the nuclear surface (corona nucleons) from the core overlap of the two nuclei (where QGP is expected to be produced), leading to an effective volume reduction of the overlap zone. In our estimates of the corona we consider the overlap of two spheres with realistic surface thicknesses. To quantify the corona, we use calculations of the nuclear overlap [47], employing the Woods-Saxon nuclear density distribution, plotted for the Au nucleus in

Fig. 4. We define the core region as corresponding to the half-density nuclear (charge) radius ($R_A=6.37$ fm for the Au nucleus) extended by a thickness X_c (see Fig. 4) and derive in this manner N_{part} and N_{coll} for the core and corona regions. The fraction of participating nucleons contained in the corona region is shown as a function of centrality in the left panel of Fig. 5 for three values of X_c : 0, 0.7 and 1.2 fm.

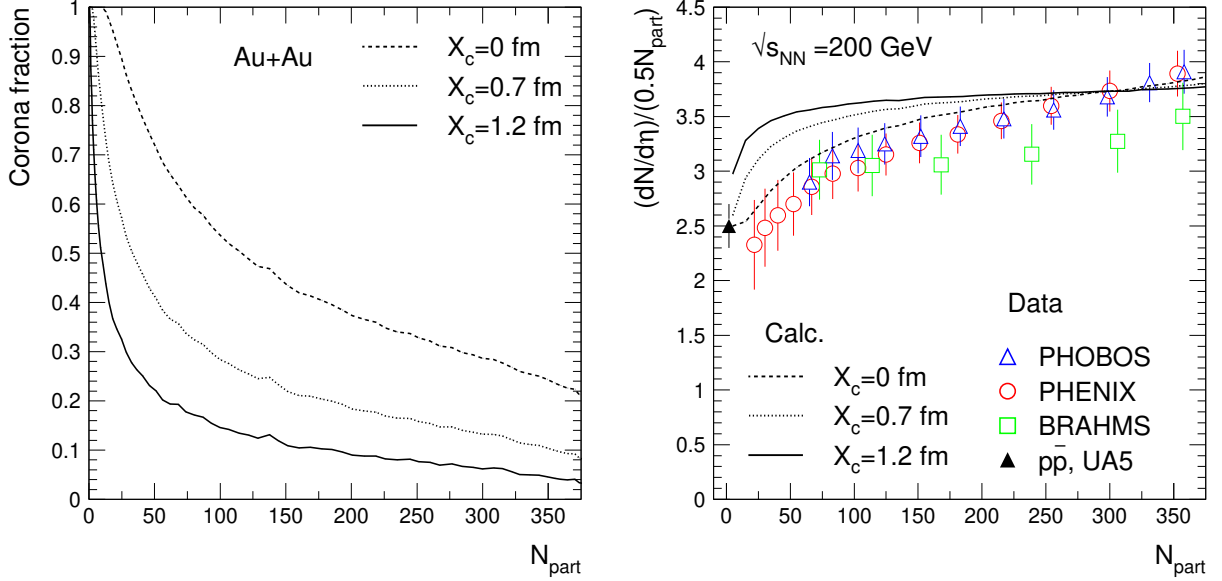


Fig. 5. Left panel: the fraction of nucleons in corona as a function of centrality. Right panel: the centrality dependence of charged particle yields at midrapidity. The data [57] are compared to estimates based on the corona contribution (the curves are arbitrarily normalized).

It was recently demonstrated [55] that the centrality dependence of particle production at RHIC and SPS can be well explained assuming an interplay of bulk production in the core and of elementary collisions in the corona part. Within this picture, we compare in the right panel of Fig. 5 our expectation for the centrality dependence of charged particle multiplicity with RHIC data from PHOBOS [56], PHENIX [57] and BRAHMS [58]. For the elementary collisions we use $dN_{ch}/d\eta=2.5$ (at midrapidity, non single-diffractive), measured in $p\bar{p}$ collisions at $\sqrt{s}=200$ GeV [59]. We normalize our calculations to the measured value [57] for $N_{part}=300$ to extract for the core $dN_{ch}/d\eta/(N_{part}/2)=4.23, 3.92$ and 3.81 for $X_c=0, 0.7$ and 1.2 fm, respectively. We conclude that this treatment of the corona effect reproduces the trend in the data only for the case $X_c=0$ which we consider somewhat extreme. However, using BRAHMS data one may come to a different conclusion. We consider $X_c=1.2$ fm a suitable choice for the extension of the core beyond R_A and in this case our calculations account for the measured centrality dependence only partially. On the other hand, the interpretation of such data within saturation ("color glass condensate") models [60,54] is quite successful. However, it is clear from the present exercise that the corona contribution needs to be considered in order to have a realistic modelling of the collision [55]. We consider for the corona thickness $X_c=1.2$ fm as a realistic value, since at that point the density has dropped to about 10 % of the central value and adopt it as a baseline choice for our following model calculations.

Based on the central values of the pQCD charm production cross sections [44,43], we show in Fig. 6 the centrality dependence of the number of $c\bar{c}$ pairs for central rapidity for the RHIC and LHC energies. In the following we perform calculations within the statistical

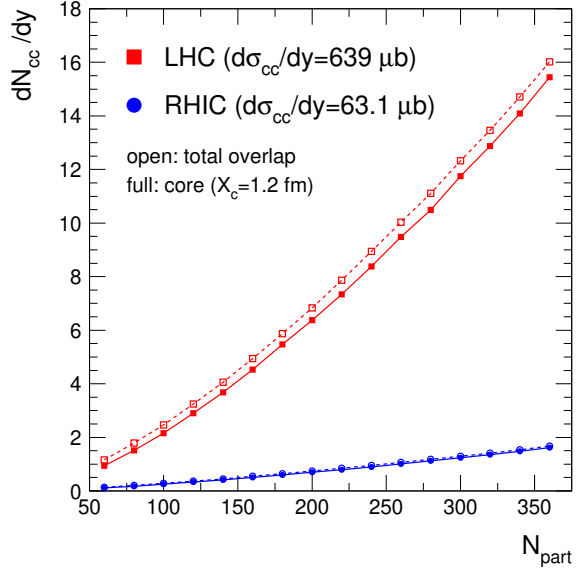


Fig. 6. Centrality dependence of rapidity density of charm yields at RHIC and LHC energies for the total overlap (open symbols) and for core only (full symbols).

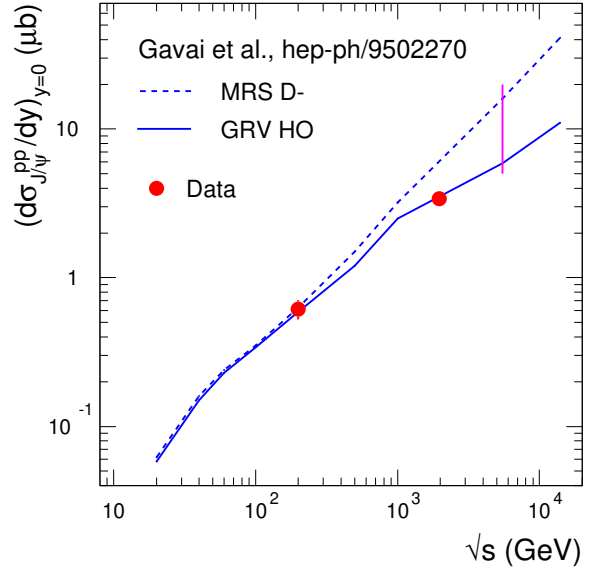


Fig. 7. Energy dependence of rapidity density of J/ψ cross section in $pp(\bar{p})$ collisions (see text for details). The LHC energy for Pb+Pb is marked by the vertical line.

hadronization model for the core, and add the contribution of the corona region for which we use the J/ψ cross section in elementary collisions. The energy dependence of the J/ψ cross section ($d\sigma/dy$) in pp collisions is shown in Fig. 7. Recent experimental data at RHIC from PHENIX [61] and at the Tevatron from CDF [62] are compared to calculations by Gavai et al. [63] for two PDFs. In our model calculations we employ for RHIC the measured [61] J/ψ cross section of $0.616 \mu\text{b}$, which is about 1% of the pQCD charm production cross section [44]. Assuming the same 1% of the calculated pQCD charm cross, for LHC we derive a J/ψ cross section of $6.39 \mu\text{b}$, which we use in the following calculations. This cross section is in line with the calculations [63] which reproduce the Tevatron data [62] (see Fig. 7). For SPS energy we employ a J/ψ cross section at midrapidity in pp collisions of 50 nb , obtained from an interpolation based on a recent compilation of data [64]. These values are summarized in Table 1.

Table 1

Summary of the values used in our calculations for charm. The values for $d\sigma_{cc}^{pp}/dy$ are from pQCD calculations, the values for $d\sigma_{J/\psi}^{pp}$ are from measurements, either interpolated (for the SPS energy, cf. ref. [64]), or directly measured at RHIC [61] or assumed as 1% of $d\sigma_{cc}^{pp}/dy$ at LHC energy.

$\sqrt{s_{NN}}$ (GeV)	$d\sigma_{cc}^{pp}/dy$ (μb)	$d\sigma_{J/\psi}^{pp}/dy$ (μb)
17.3	$5.7^{+5.7}_{-2.8}$	0.050 ± 0.030
200	$63.7^{+95.6}_{-42.3}$	0.616 ± 0.093
5500	639^{+639}_{-319}	6.4 ± 3.2

The yield of J/ψ mesons, e.g., is then calculated as follows:

$$N_{J/\psi} = N_{J/\psi}^{core} + N_{J/\psi}^{corona} \quad (2)$$

where

$$N_{J/\psi}^{core} = g_c^2 n_{J/\psi}^{th} V^{core} \quad (3)$$

and

$$N_{J/\psi}^{corona} = N_{coll}^{corona} \sigma_{J/\psi}^{pp} / \sigma_{inel}^{pp}. \quad (4)$$

and we use for σ_{inel}^{pp} values of 30, 42, and 60 mb at SPS, RHIC, and LHC energies, respectively.

The $\Upsilon(1S)$ cross section in pp collisions at the LHC energy is assumed to be 36.8 nb, which is $1.7 \cdot 10^{-3}$ of the $b\bar{b}$ cross section at $\sqrt{s_{NN}}=5.5$ TeV. This is the fraction derived from the Tevatron data at 1.8 TeV [62,65,66].

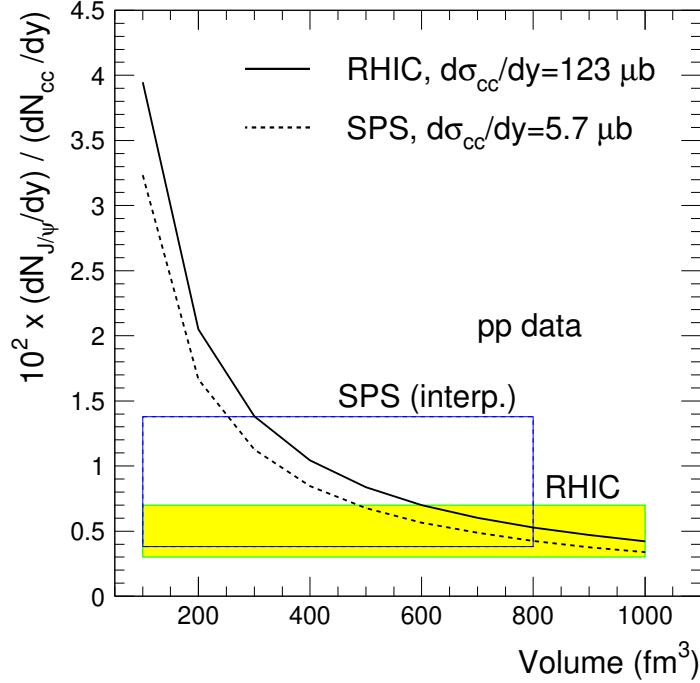


Fig. 8. Volume dependence of the rapidity density of the J/ψ yield calculated within the SHM, normalized to the $c\bar{c}$ yield. The measured value for the RHIC energy [61,49] is indicated by the shaded band, while the open box depicts the interpolated value for the SPS energy.

Before proceeding to discuss our calculations for nucleus-nucleus collisions, we investigate the model predictions for the proton-proton case. In Fig. 8 we show the volume dependence of the predicted J/ψ yield normalized to the $c\bar{c}$ yield. It is seen that, for a realistic volume expected for pp collisions, of about 30-50 fm^3 , the model strongly overestimates the measured [61,49] or interpolated [64] values for the RHIC and SPS energies, respectively. This is expected, as charm quarks are not likely to thermalize for small volumes. As a consequence, we consider, somewhat schematically, the volume for which the model calculations reach the measured values in pp collisions to be the minimal core volume required for the validity of our model. Based on the results shown in Fig. 8, we adopt

the value $V_{QGP}^{min}=400 \text{ fm}^3$. Below this value, we consider that the J/ψ production takes place exclusively via hard processes in elementary collisions. In nature, the transition from the QGP region to the pp region is likely to be continuous, but we have no quantitative means to model this transition. Also, from Fig. 8 it is clear that V_{QGP}^{min} carries a rather large uncertainty. In addition, we do not consider the experimental fluctuations in the centrality selection which would further smoothen the transition.

3 Annihilation of charm quarks in the QGP

In this section we investigate the assumption, central to our model, that the number of \bar{c} and c quarks which are produced in initial hard collisions stays constant during the evolution of the QGP until the critical temperature T_c is reached and the system hadronizes. For such an estimate we assume that the light quarks and gluons reach equilibrium to form a QGP relatively quickly after the first hard collisions, on a time scale of the order of 1 or at most a few fm/c . We first note that further production of $\bar{c}c$ pairs in the QGP can be completely neglected at temperatures $T < 1 \text{ GeV}$ [21], as the charm quarks are far from chemical equilibrium. On the other hand, charm quark annihilation may take place via reactions of the type

$$c + \bar{c} \rightarrow g + g \tag{5}$$

or

$$c + \bar{c} \rightarrow q + \bar{q}, \tag{6}$$

or via more complex reactions such as those forming 3 or more gluons, a quark-antiquark pair plus gluons, etc. Within the framework of perturbative QCD, the cross sections for Eqs. 5, 6 can be evaluated. In the following, we perform such an evaluation for Eq. 5 and use it to determine the annihilation rate of charm quark pairs in the QGP via this channel. Since the 2-gluon annihilation is the dominant channel, it's cross section significantly exceeding all other listed cross sections [67], we take this estimate as an indication of the total charm annihilation in the QGP.²

To evaluate the total annihilation rate we start from the rate equation

$$\frac{dr_{c\bar{c}}}{d\tau} = n_c n_{\bar{c}} \langle \sigma_{c\bar{c} \rightarrow gg} v_r \rangle, \tag{7}$$

where $\langle \sigma_{c\bar{c} \rightarrow gg} v_r \rangle$ is the thermal average of the annihilation cross section times the relative velocity v_r in the QGP, and $n_c = n_{\bar{c}}$ is the charm quark density. The quantity $\frac{dr_{c\bar{c}}}{d\tau}$ is the annihilation rate per volume or the rate of change of the charm quark density. The cross section for Eq. 5 is taken to first order in the strong coupling constant α_s from the

² Channels with 3 or more gluons should be suppressed if gluons acquire, as expected, a thermal mass in the QGP.

work of [68], where the inverse cross section for $g + g \rightarrow c + \bar{c}$ is computed, applying detailed balance. To get an estimate of the upper limit for this cross section in the QGP we evaluate the equation of [68] using $\alpha_s = 1$ and for a charm quark mass of $m_c = 1.5$ GeV.

The charm quark density n_c depends on the evolution time of the QGP, i.e.

$$n_c = \frac{dN_c/dy(\tau)}{V(\Delta y = 1, \tau)} \leq \frac{dN_c/dy(\tau_0)}{V(\Delta y = 1, \tau)}, \quad (8)$$

where τ_0 is the initial time of QGP formation and dN_c/dy is the charm quark rapidity density.

The total annihilation yield of charm quarks in the QGP is then given by

$$N_{c\bar{c}}^{anni} = \int_{\tau_0}^{\tau_c} \frac{dr_{c\bar{c}}}{d\tau} V(\Delta y = 1, \tau) d\tau. \quad (9)$$

To proceed further we need to model the evolution of the QGP. In the spirit of our upper limit estimate we assume here a 1-dimensional Bjorken-type expansion of the QGP yielding, using entropy conservation, a relation between T and τ :

$$\frac{\pi^2}{45} (32 + 21N_f) T^3 \tau = 3.8 \frac{dN/dy}{A_\perp}, \quad (10)$$

where N_f is the (effective) number of massless flavors, and dN/dy is the total particle rapidity density. The transverse system size A_\perp is about 150 fm² at T_c for central Au-Au or Pb-Pb collisions. Using this scenario we get for the temporal evolution of the volume then

$$V(\Delta y = 1, \tau) = A_\perp \tau. \quad (11)$$

The total annihilation yield of charm quarks in the QGP is, using Eqs. 8,9,11, given by

$$N_{c\bar{c}}^{anni} \leq \left(\frac{dN_c}{dy}(\tau_0) \right)^2 \frac{1}{A_\perp} \int_{\tau_0}^{\tau_c} \frac{d\tau}{\tau} \langle \sigma_{c\bar{c} \rightarrow gg} v_r \rangle. \quad (12)$$

In the following we consider 2 scenarios (assuming $N_f = 2.2$ and $\tau_0 = 1$ fm for both): i) at RHIC energy, this leads to $\tau_c = 2.7$ fm and to an initial temperature $T(\tau_0) = 225$ MeV for a charged particle rapidity density of 660 and ii) the LHC energy scenario results in $\tau_c = 8.3$ fm and $T(\tau_0) = 325$ MeV for a charged particle rapidity density of 2000. Following [69] we evaluate the temperature dependence of the thermal average in Boltzmann approximation. The resulting temperature dependence of the thermal average is presented in Fig. 9. Since the charm quark annihilation cross section decreases with increasing scale (\sqrt{s}), the resulting thermal average also drops with increasing temperature.

To get numerical results on the annihilation rate we determine the integral in Eq. 12 for both scenarios numerically. Note that the lifetime of the QGP enters (to 1st order) only logarithmically, implying that the details of the expansion are not very important for our estimate. In particular, using much smaller values for τ_0 and correspondingly higher initial temperatures changes the results only marginally. We furthermore add that the volume used here for an upper limit on the annihilation yield is computed when the system reaches T_c . Taking into account the increase of volume until chemical freeze-out, which is used in the next section, would further decrease the annihilation yield and, hence, is not considered here.

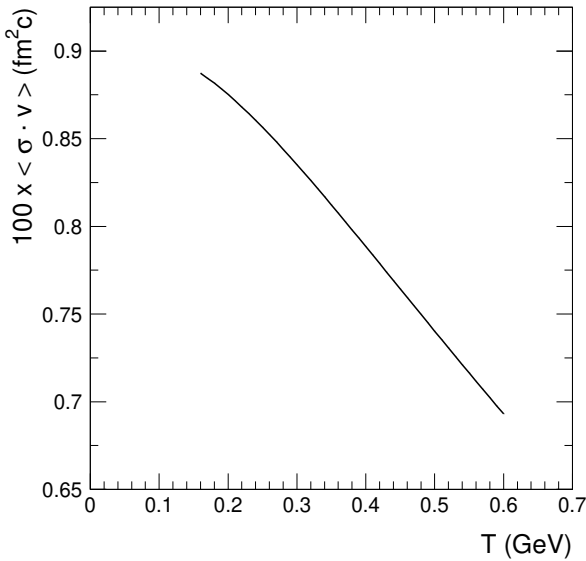


Fig. 9. Temperature dependence of the thermal average as defined in Eq. 7 (see text).

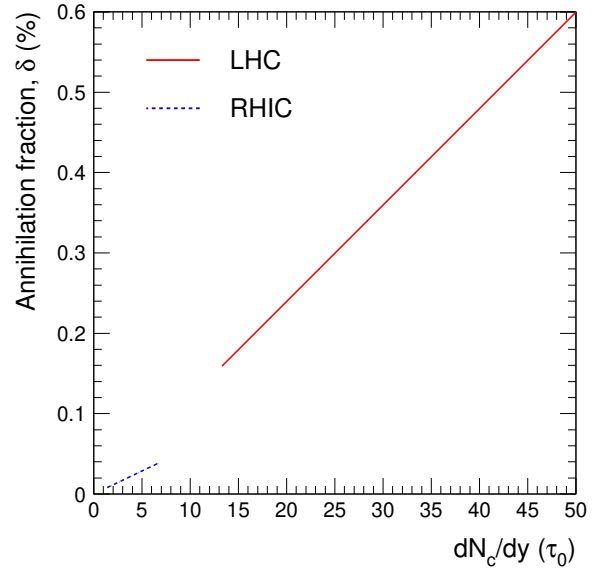


Fig. 10. Annihilation rate as a function of initial charm rapidity density.

The final results of the estimate for the fraction of charm quarks lost via annihilation, $\delta = N_{c\bar{c}}^{anni}/dN_c/dy(\tau_0)$ are given in Fig. 10 for the RHIC and LHC scenarios. Since the annihilation yields increase quadratically with the charm quark rapidity density we start, in the spirit of an upper limit estimate, the calculation at the values predicted by pQCD calculations for each scenario, i.e. $\frac{dN_c}{dy}(\tau_0) = \frac{dN_c^{pQCD}}{dy} = 1.4$ and 13.3, and then increase these numbers by up to a factor 5.

In general, the fraction of annihilating $c\bar{c}$ pairs in the QGP is negligible for both scenarios. Even for an unrealistically high value of $\frac{dN_c}{dy}(\tau_0) \approx 60$ in the LHC scenario, the total fraction of annihilated pairs is less than 1%, and decreases linearly for lower charm quark densities. For realistic scenarios our estimate implies that charm quark annihilation in the plasma can be safely neglected. Along the same line, production of charmonia via uncorrelated charm quark annihilation in the QGP is expected to fall significantly below the above computed annihilation yield into gluons, lending strong support to our interpretation that all quarkonia are produced late, when the system reaches the critical temperature and hadronizes.

This result has a number of significant consequences. We first note that the small annihilation rate in the plasma also implies that charmonia are not likely to be formed in the

plasma. Therefore, the possible existence of (quasi-)bound J/ψ mesons in the QGP [70,19] would not influence our predictions for charmonia yields as these states would never be populated during the evolution of the QGP. We neglect in this context J/ψ production in hard collisions before QGP formation, i.e. before τ_0 , because of the the large formation time [71].

These considerations also highlight the differences between our approach, where all charmonia are formed non-perturbatively at T_c , during hadronization of the QGP, and the recombination model of [7,8], where the cross section for the production of J/ψ mesons from c and \bar{c} quarks is obtained by first computing, using the operator product expansion technique [72], the dissociation of J/ψ mesons due to collisions with gluons and then inverting this cross section using detailed balance. We note that this procedure yields a cross section for J/ψ production of several mb [9], significantly exceeding that for annihilation of the $c\bar{c}$ pair into 2 gluons, see Eq. 5.

4 Centrality and rapidity dependence of quarkonia yields

In our earlier studies [1,5] we have shown that the J/ψ data at SPS energy can be described within the statistical approach, but only when assuming that the charm production cross section is enhanced by about a factor of 3 beyond the perturbative QCD (pQCD) predictions. Those results were obtained assuming that hadronization of charm takes place in the whole volume of the system at chemical freezeout. We consider this assumption to be rather extreme and adopt here a picture of hadronization within one unit of rapidity at midrapidity, as done for the analysis of the yields of hadrons without charm within the thermal model [36,38]. The comparison of our model calculations with the data measured at SPS by the NA50 experiment is shown in Fig. 11. Two sets of data are included in Fig. 11: the NA50 data of 1998, as analyzed by Gosset et al. [73] and with a further normalization (see [1]) and the NA50 data of 2004 [74], representing the yield of J/ψ normalized to the Drell-Yan yield, which we arbitrarily normalize for the sake of comparison, assuming that the Drell-yan yield scales with N_{coll} . It is seen that the two data sets show a very good consistency in the centrality dependence. Note that a factor of 0.5 was used to convert the full phase space experimental data [73,1], to midrapidity yields.

The experimental data are well described by invoking a moderate enhancement of the charm production cross section of a factor of 2 compared to pQCD calculations [43]. Very clearly, adopting for the present calculations the hadronization within one unit of rapidity leads to an agreement with the data for a smaller enhancement of the charm cross section than required in our earlier study [5]. New measurements by the NA60 experiment [76] indicate that the enhancement in the dimuon yield below the J/ψ mass, earlier observed by the NA50 [77], is of prompt origin and, as such, cannot be interpreted as an enhancement of the charm production cross section, although an experimental result on the charm cross section is currently not available. We also note that a factor of 2 enhancement is within uncertainties of the pQCD calculations.

A comparison between calculations and data [75] is shown in the right panel of Fig. 11 for the centrality dependence of the yield of ψ' relative to J/ψ . Using the present core and

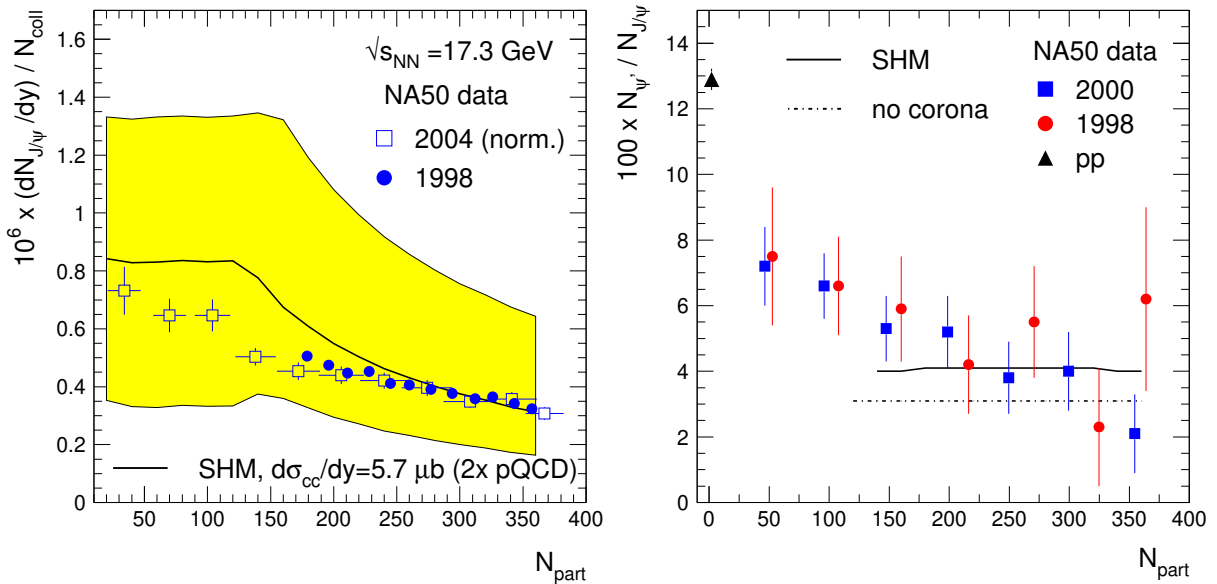


Fig. 11. Centrality dependence of J/ψ yield per number of collisions (left panel) and of the ratio of yields of ψ' and J/ψ (right panel) at the SPS energy. The shaded band in the left panel denotes the range in the charm production cross section (a factor of 2 up and down) and the error assumed for the J/ψ cross section in pp collisions. The experimental data on J/ψ yield are from ref. [73] (see [1]) and ref. [74] (2004 NA50 data) and on the $\psi'/J/\psi$ ratio from ref. [75].

corona model leads to a 25% increase of the ratio compared to the case when all nucleons are considered to be part of the QGP region (no corona). The model predictions are shown only down to the N_{part} values corresponding to V_{QGP}^{min} . For more peripheral collisions the data suggest a continuous transition towards the value measured in elementary collisions.

For RHIC energy, the centrality dependence of the J/ψ rapidity density at midrapidity is shown in Fig. 12, considering three cases for the charm production cross section: i) as calculated in pQCD [44], and as measured by ii) PHENIX [49] and iii) STAR [48]. The model calculations agree with the recent preliminary PHENIX data [14] very well for the central value of the pQCD charm production cross section, in line with our earlier comparison [5]. The yield is scaled by the number of binary collisions, N_{coll} . In this scaled representation the model predicts a slight decrease of the J/ψ yield as a function of N_{part} , a trend which is compatible with the data. The model overestimates the data by about a factor of 2 for the central value of the charm production cross section measured by PHENIX [49], but is compatible with the data for the lower limit of this measured cross section. If we use the values of the charm cross section measured by STAR [48] the model overestimates the data by about a factor of 10 and is clearly incompatible with the data also concerning the trend as a function of centrality.

Note that the steps in the calculations seen around $N_{part}=70$ are the outcome of the sharp transition from the core region to the pp region below $V_{QGP}^{min}=400 \text{ fm}^3$. As we have mentioned earlier, this transition is probably continuous, but we have not tried at this stage to model it.

The rapidity dependence of the J/ψ yield is shown in Fig. 13 for two centrality bins for

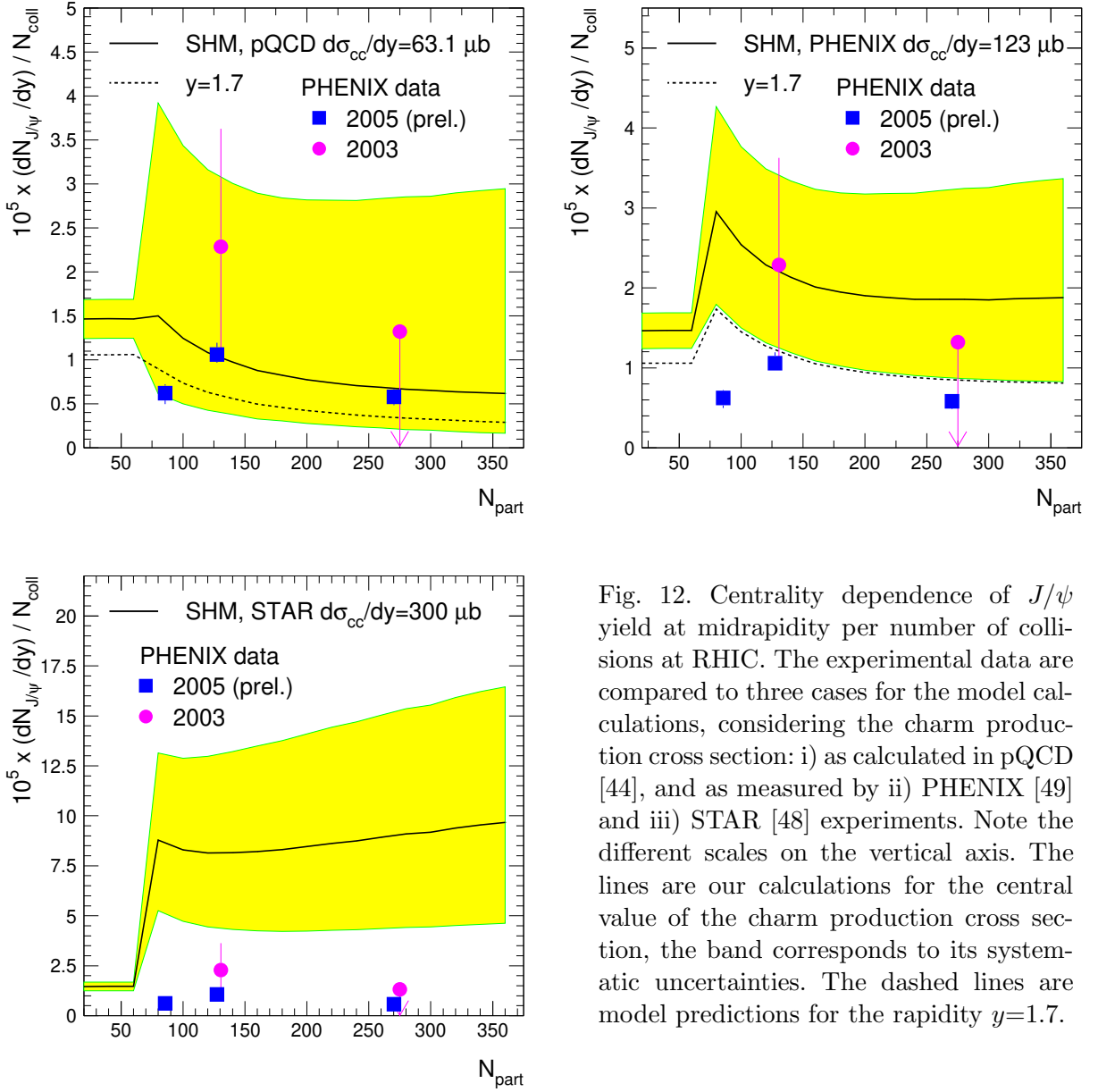


Fig. 12. Centrality dependence of J/ψ yield at midrapidity per number of collisions at RHIC. The experimental data are compared to three cases for the model calculations, considering the charm production cross section: i) as calculated in pQCD [44], and as measured by ii) PHENIX [49] and iii) STAR [48] experiments. Note the different scales on the vertical axis. The lines are our calculations for the central value of the charm production cross section, the band corresponds to its systematic uncertainties. The dashed lines are model predictions for the rapidity $y=1.7$.

Au-Au collisions. The preliminary PHENIX data [14] are well described by the model calculations for the central value of the pQCD charm cross section. In particular, the narrow rapidity distributions predicted within the kinetic recombination model [9] are not observed here because of the rather broad rapidity distribution of the charm production cross section [45].

The model predictions for the centrality and rapidity dependence of J/ψ production at LHC are shown in Fig. 14. For most of the range of the charm production cross section considered, a growth with centrality faster than that of the number of binary collisions is seen in the J/ψ yield, allowing to make a distinct case for the statistical hadronization scenario at LHC. This increase is stronger for larger charm cross section values. The rapidity distribution is broader than at RHIC energy. As a consequence, the measured rapidity densities of J/ψ in the ALICE central barrel ($|\eta| < 0.9$) and in the muon spectrometer ($\eta = 2.5 - 4.0$) are expected to be comparable.

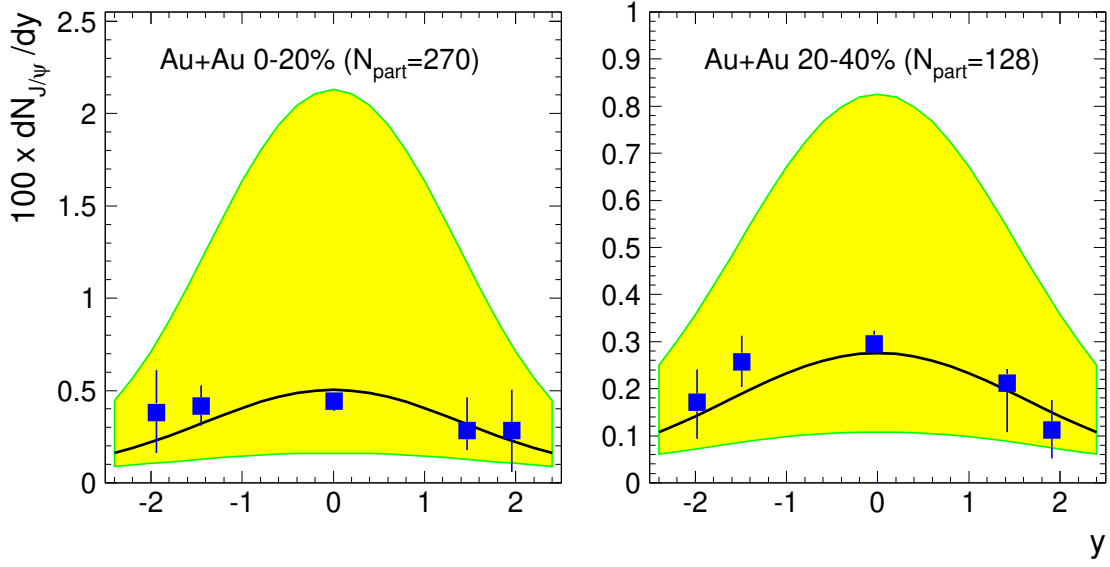


Fig. 13. Rapidity dependence of the J/ψ yield at RHIC for two centrality bins. The SHM calculations, performed for the nominal pQCD charm production cross section (continuous line with the band denoting the systematic errors of the cross section) are compared to preliminary PHENIX data [14].

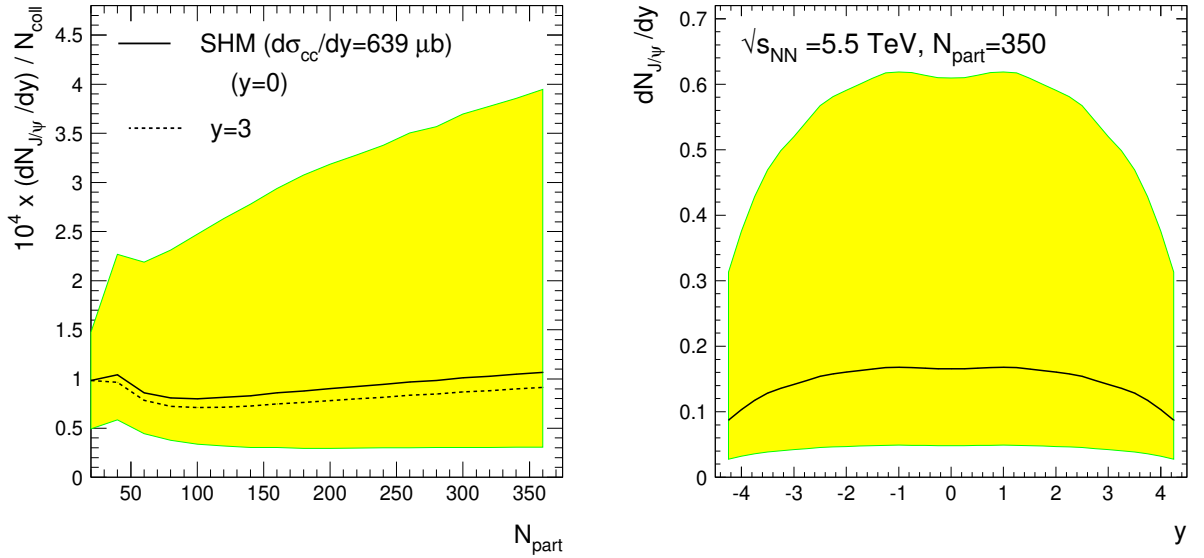


Fig. 14. Predictions for the J/ψ rapidity density at LHC. Left panel: centrality dependence (normalized to N_{coll}) at midrapidity, right panel: rapidity dependence for central collisions ($N_{part}=350$).

The model predictions for the centrality and rapidity dependence of Υ production at LHC are shown in Fig. 15. A decrease as a function of centrality is seen (note again the normalization to N_{coll}), similar to the one observed for J/ψ at RHIC.

Fig. 16 shows a comparison of the calculated J/ψ yield per number of $c\bar{c}$ pairs for RHIC and LHC energies. This figure illustrates the succinct change in trend expected for measurements at LHC energy, due to the strong increase with energy of the total charm

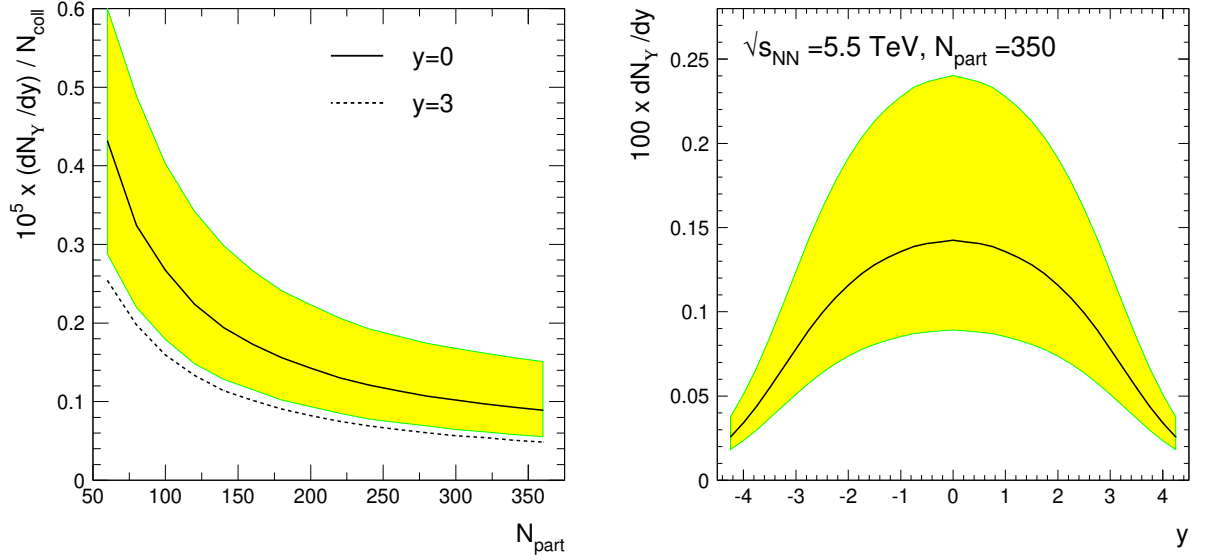


Fig. 15. Yield of Υ at LHC. Left panel: centrality dependence for $y=0$ (continuous line with error band for the uncertainty of bottom cross section) and $y=3$ (dashed line). Right panel: rapidity dependence for central collisions ($N_{\text{part}}=350$).

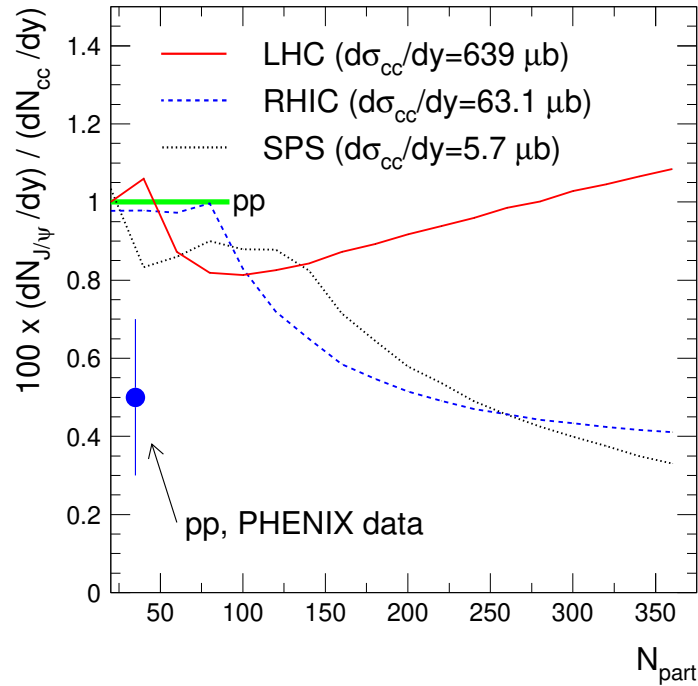


Fig. 16. Centrality dependence of J/ψ yield normalized to $c\bar{c}$ yield for the SPS, RHIC and LHC energies. The thick line is the value used in the model for pp collisions. The dot corresponds to the PHENIX measurements in pp collisions at RHIC energy.

production cross section. Note, in particular the decrease with centrality of the J/ψ yield at RHIC, originating from the canonical suppression of the open charm hadrons. The dot corresponds to the PHENIX measurement of J/ψ production in pp collisions [61] normalized to the $c\bar{c}$ cross section, also measured by PHENIX [49]. This value is smaller than

the value of 1% derived using the pQCD value [44] for the charm cross section and much smaller than the value of 2.5% derived earlier by Gavai et al. [63].

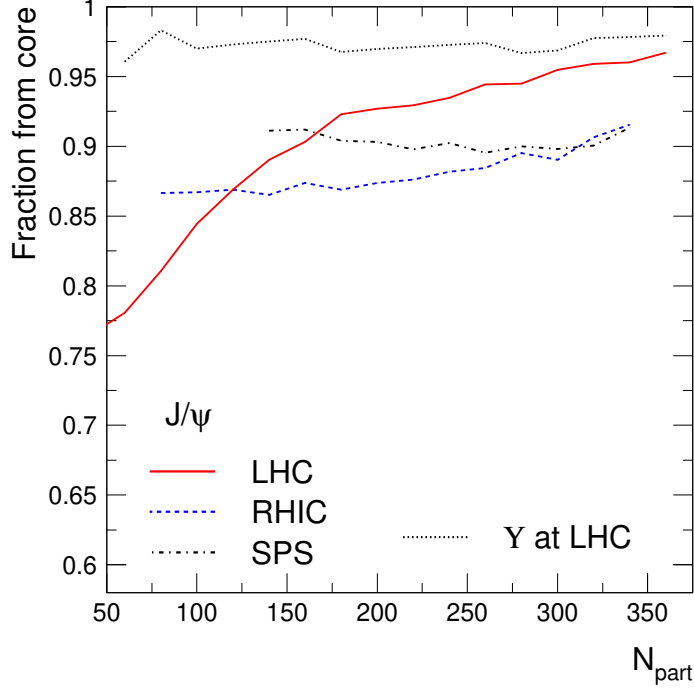


Fig. 17. Centrality dependence of the fraction of yields of J/ψ and Υ from the core (QGP) region relative to the total overlap.

In Fig. 17 we present the fraction of J/ψ and of Υ yields from the core (QGP) region relative to the total (core and corona) overlap. For the J/ψ yields, this contribution of corona to the total J/ψ yield is moderate for all the three energies. Note as well the different centrality dependences for the three energy regimes. The Υ yield is predominantly originating from the core part.

5 Transverse momentum dependence

We turn now to the analysis of the transverse momentum (p_t) spectrum of J/ψ mesons. Within our model, the p_t distribution of J/ψ , as well as of any hadron carrying charm (or beauty), is determined by the temperature and transverse expansion velocity, β , at chemical freeze-out. We employ a formula for collective expansion [78], but consider, to keep the input minimal, one average velocity instead of a velocity profile:

$$\frac{dN}{p_t \cdot dp_t} \sim m_t \cdot I_0\left(\frac{p_t \sinh y_t}{T}\right) \cdot K_1\left(\frac{p_t \cosh y_t}{T}\right) \quad (13)$$

where $m_t = \sqrt{m_0^2 + p_t^2}$, m_0 is the rest mass of the particle, and $y_t = \tanh^{-1}(\beta)$, with β the collective (transverse) expansion velocity in units of the speed of light. The I_0 and K_1

are the modified Bessel functions.

Our picture is similar to that proposed and tested with data at the SPS by Gorenstein et al. [79]. Spectra of both J/ψ and ψ' mesons and of Ω hyperons were shown [79] to be described by a (kinetic) temperature equal to the chemical freeze-out temperature, while the expansion velocity was found to be substantially lower than for the other hadrons. This indeed suggests a kinetic freeze-out of J/ψ coincident with the chemical freeze-out (at the phase boundary between QGP and hadronic matter [38]), with β characterizing the transverse expansion in the QGP phase.

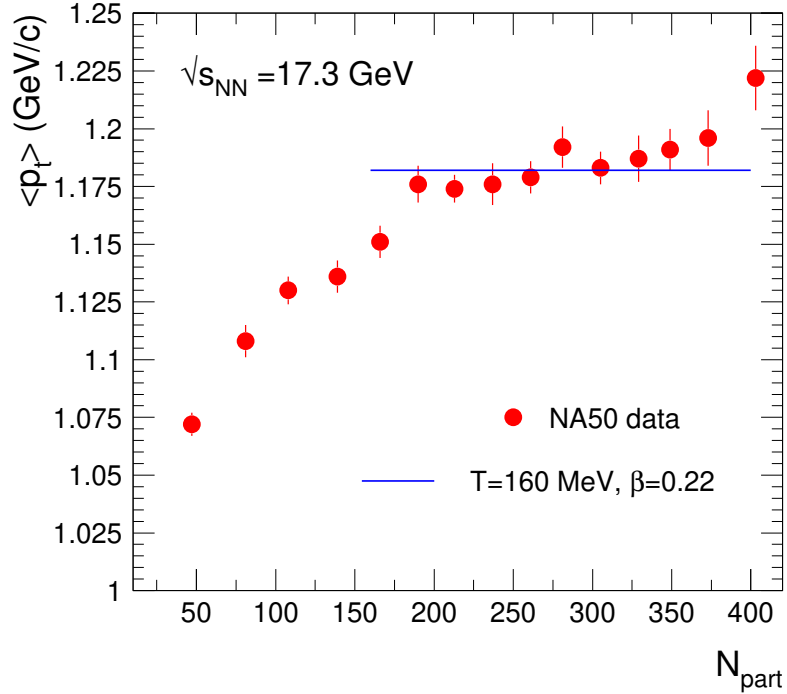


Fig. 18. Centrality dependence of the average transverse momentum of J/ψ mesons in Pb-Pb collisions at SPS energy. The data measured by the NA50 experiment [80] are compared to calculations using Eq. 13.

To check the validity of this interpretation, we calculate with Eq. 13 the transverse momentum spectrum of J/ψ and compare it to the available data. For SPS energy we compare the centrality dependence of the average transverse momentum of J/ψ to the NA50 data [80] in Fig. 18. The data are well described by the calculations using $T=160$ MeV and $\beta=0.22$, in agreement with the earlier results [79]. Note that the data approach a constant value for central collisions ($N_{part} > 150$), where the present model is applicable. We would like to emphasize that the $\langle p_t \rangle$ data cannot constrain T and β in a satisfactory way. When fitting the data, local minima are present in the χ^2 distribution. Several sets of T and β values describe the data equally well, as known from fits of distributions of other hadron species [81]. This problem may be alleviated if high-precision spectra as a function of centrality become available.

For RHIC energy we calculate the J/ψ spectrum taking into account both the QGP contribution (according to Eq. 13) and the corona part. For the corona, we use the spectrum measured in pp collisions [83], which we fit in order to be able to interpolate or extrapolate.

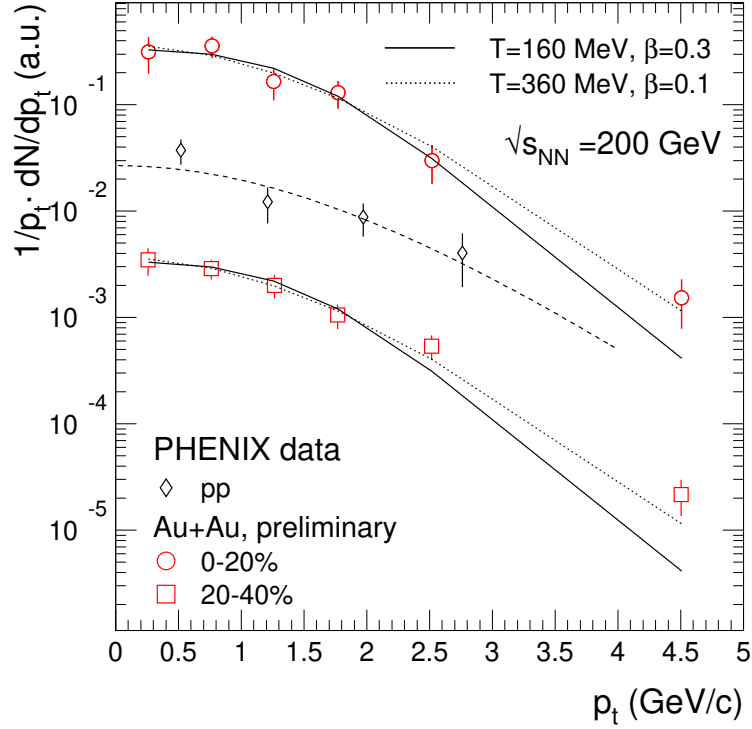


Fig. 19. Transverse momentum distribution of J/ψ in Au-Au collisions at RHIC energy [82]. The data (symbols) are compared with calculations using Eq. 13 for two cases of the kinetic freezeout parameters (lines). The spectrum measured in pp collisions [83] with the fit as used for the corona part in our calculations is also shown.

Fig. 19 we show the comparison of the J/ψ spectra measured by the PHENIX experiment [82] with our calculations. Two sets of parameters are investigated for the QGP part: i) $T=160$ MeV, $\beta=0.3$ and ii) $T=360$ MeV, $\beta=0.1$. The data are well compatible with the picture of J/ψ production via hadronization at chemical freeze-out, expected to be described by scenario i), but the data are not precise enough at this stage to exclude scenario ii). Interestingly, the expansion velocity extracted from fits of the spectra of Ω and ϕ particles, which are also expected to interact rather weakly in the hadronic stage, yields for $T = 160$ MeV $\beta \simeq 0.4-0.5$, somewhat larger than obtained for the charmonia, but significantly lower than β values determined for other hadrons [81].

In Fig. 20 we present predictions for the transverse momentum spectrum of J/ψ and Υ in central collisions at LHC. We show the spectra for a range of expansion velocities, as expected for LHC energy. For pp collisions in the corona we have assumed the same spectral shape at LHC as measured in $p\bar{p}$ collisions at Tevatron [62], which are also included for comparison in Fig. 20. The corona fractions corresponding to central Pb+Pb collisions ($N_{part}=350$) are 0.13 for J/ψ and 0.09 for Υ . For both J/ψ and Υ , the spectral shapes expected within the statistical hadronization model are very different compared those expected from the superposition of pp collisions, making the data at LHC a stringent test of our model.

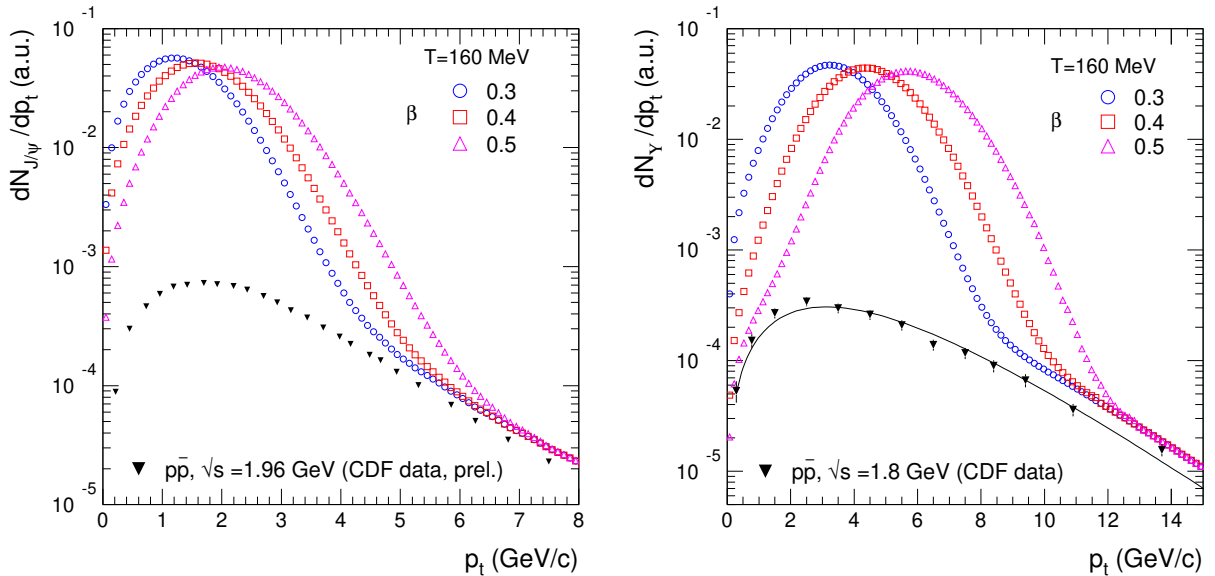


Fig. 20. Predictions for momentum spectrum of J/ψ (left panel) and Υ (right panel) for different values of the expansion velocity, β , for central Pb+Pb collisions ($N_{part}=350$). Also included are the measured spectra in $p\bar{p}$ collisions at Tevatron [62].

6 Conclusions

We have presented new results on the statistical hadronization of heavy quarks at the SPS, RHIC and LHC energies. We have focused on the results for J/ψ yields, but have also extended the model to predict Υ yields in Pb+Pb collisions at the LHC energy. Included in our model is now a separation of the collision geometry into a core (QGP) and a corona (pp collisions) part. Our estimate of the annihilation rates of charm quark in a hot plasma demonstrates that this is a small effect. An important ingredient in our model is the charm production cross section, which is presently quite poorly measured. We have considered the effect of its uncertainty on the model predictions. For SPS energy, our present calculations are performed assuming that the hadronization takes place within one unit of rapidity at midrapidity, as used also for RHIC and LHC energies. Good agreement with data is found with a charm cross section which is moderately (a factor of 2) larger, but consistent within errors with pQCD calculations. For RHIC energy we have studied the centrality and rapidity dependence of J/ψ production. Our model is in good agreement with the available preliminary data, lending strong support for the picture of statistical hadronization. We have discussed the transverse momentum distributions of J/ψ mesons expected from the model. The present data, in particular those at RHIC energy, are compatible with the picture of the J/ψ (kinematic) freeze-out coincident with chemical freeze-out, but more precise data are needed to quantitatively explore this idea. Our predictions for LHC energy concerning centrality, rapidity and transverse momentum dependence of the J/ψ yield will be tested with data within the next few years.

Acknowledgments

We are indebted to M. Cacciari for providing us the rapidity distribution of the charm production cross section at the RHIC energy and for valuable discussions.

K. Redlich acknowledges the support from the Polish Committee of Scientific Research KBN under grant 2P03 (06925).

References

- [1] P. Braun-Munzinger, J. Stachel, Phys. Lett. B 490 (2000) 196 [nucl-th/0007059]; Nucl. Phys. A 690 (2001) 119c [nucl-th/0012064].
- [2] M.I. Gorenstein, A.P. Kostyuk, H. Stöcker, W. Greiner, Phys. Lett. B 509 (2001) 277 [hep-ph/0010148]; Phys. Lett. B 524 (2002) 265 [hep-ph/0104071]
- [3] L. Grandchamp, R. Rapp, Phys. Lett. B 523 (2001) 60 [hep-ph/0103124]; Nucl. Phys. A 709 (2002) 415 [hep-ph/0205305].
- [4] A.P. Kostyuk, M.I. Gorenstein, H. Stöcker, W. Greiner, Phys. Lett. B 531 (2002) 195 [hep-ph/0110269]; Phys. Rev. C 68 (2003) 041902 [hep-ph/0305277].
- [5] A. Andronic, P. Braun-Munzinger, K. Redlich, J. Stachel, Phys. Lett. B 571 (2003) 36 [nucl-th/0303036].
- [6] E.L. Bratkovskaya, A.P. Kostyuk, W. Cassing, H. Stöcker, Phys. Rev. C 69 (2004) 054903 [nucl-th/0402042].
- [7] R.L. Thews, M. Schroedter, J. Rafelski, Phys. Rev. C 63 (2001) 054905 [hep-ph/0007323].
- [8] R.L. Thews, AIP Conf. Proc. 631 (2002) 490 [hep-ph/0206179].
- [9] R.L. Thews, M.L. Mangano, Phys. Rev. C 73 (2006) 014904 [hep-ph/0505055].
- [10] L. Grandchamp, S. Lumpkins, D. Sun, H. van Hees, R. Rapp, Phys. Rev. C 73 (2006) 064906 [hep-ph/0507314].
- [11] F. Becattini, Phys. Rev. Lett. 95 (2005) 022301 [hep-ph/0503239].
- [12] S.S. Adler et al. (PHENIX), Phys. Rev. C 69 (2004) 014901 [nucl-ex/0305030].
- [13] A. Tai (STAR), J. Phys. G 30 (2004) S809 [nucl-ex/0404029].
- [14] H. Pereira Da Costa (PHENIX), Nucl. Phys. A 774 (2006) 747 [nucl-ex/0510051].
- [15] P. Crochet, Eur. Phys. J. C 43 (2005) 437 [nucl-ex/0503008]; nucl-ex/0510017.
- [16] P. Crochet, Nucl. Phys. A 715 (2003) 359 [nucl-ex/0209011].
- [17] T. Matsui, H. Satz, Phys. Lett. B 178 (1986) 416.
- [18] H. Satz, hep-ph/0609197.
- [19] M. Asakawa, T. Hatsuda, Phys. Rev. Lett. 92 (2004) 012001 [hep-lat/0308034].

- [20] K. Petrov, A. Jakovac, P. Petrecky, A. Velytsky, PoS LAT2005 (2006) 153 [hep-lat/0509138].
- [21] P. Braun-Munzinger, K. Redlich, Eur. Phys. J. C 16 (2000) 519 [hep-ph/0001008].
- [22] S. Batsouli, S. Kelly, M. Gyulassy, J.L. Nagle, Phys. Lett. B 557 (2003) 26 [nucl-th/0212068].
- [23] Z.-W. Lin, D. Molnar, Phys. Rev. C 68 (2003) 044901 [nucl-th/0304045].
- [24] V. Greco, C. M. Ko, R. Rapp, Phys. Lett. B 595 (2004) 202 [nucl-th/0312100].
- [25] G.D. Moore, D. Teaney, Phys. Rev. C 71 (2005) 064904 [hep-ph/0412346].
- [26] X. Zhu, P. Zhuang, N. Xu, Phys. Lett. B 607 (2005) 107 [nucl-th/0411093].
- [27] B. Zhang, nucl-th/0606039.
- [28] S.S. Adler et al. (PHENIX), Phys. Rev. C 72 (2005) 024901 [nucl-ex/0502009].
- [29] M. Djordjevic, M. Gyulassy, S. Wicks, Phys. Rev. Lett. 94 (2005) 112301 [hep-ph/0410372].
- [30] S.S. Adler et al. (PHENIX), Phys. Rev. Lett. 96 (2006) 032301 [nucl-ex/0510047].
- [31] J. Bielcik (STAR), nucl-ex/0511005.
- [32] M. Djordjevic, M. Gyulassy, R. Vogt, S. Wicks, Phys. Lett. B 632 (2006) 81 [nucl-th/0507019].
- [33] H. van Hees, R. Rapp, Phys. Rev. C 71 (2005) 034907 [nucl-th/0412015]; H. van Hees, V. Greco, R. Rapp, hep-ph/0601166.
- [34] B. Zhang, L.W. Chen, C.M. Ko, Phys. Rev. C 72 (2005) 024906 [nucl-th/0502056].
- [35] D. Molnar, nucl-th/0608069.
- [36] P. Braun-Munzinger, I. Heppe, J. Stachel, Phys. Lett. B 465 (1999) 15 [nucl-th/9903010].
- [37] P. Braun-Munzinger, D. Magestro, K. Redlich, J. Stachel, Phys. Lett. B 518 (2001) 41 [hep-ph/0105229].
- [38] A. Andronic, P. Braun-Munzinger, J. Stachel, Nucl. Phys. A 772 (2006) 167 [nucl-th/0511071].
- [39] J. Adams et al. (STAR) Phys. Rev. Lett. 92 (2004) 112301 [nucl-ex/0310004].
- [40] W.-M. Yao et al., J. Phys. G 33 (2006) 1 [<http://pdg.lbl.gov/>].
- [41] M.A. Nowak, Int. J. Mod. Phys. A 20 (2005) 229 [hep-ph/0407272].
- [42] I. Arsene et al. (BRAHMS), Nucl. Phys. A 757 (2005) 1 [nucl-ex/0410020].
- [43] R. Vogt, Int. J. Mod. Phys. E 12 (2003) 211 [hep-ph/0111271].
- [44] M. Cacciari, P. Nason, R. Vogt, Phys. Rev. Lett. 95 (2005) 122001 [hep-ph/0502203].
- [45] M. Cacciari, private communication.
- [46] ALICE Collaboration, J. Phys. G: Nucl. Part. Phys. 30 (2004) 1517.
- [47] D. Miśkowiec, <http://www.gsi.de/~misko/overlap/>.
- [48] J. Adams et al. (STAR), Phys. Rev. Lett. 94 (2005) 062301 [nucl-ex/0407006].

- [49] A. Adare et al. (PHENIX), hep-ex/0609010.
- [50] S.S. Adler et al. (PHENIX), Phys. Rev. Lett. 94 (2005) 082301 [nucl-ex/0409028].
- [51] D. Acosta et al. (CDF), Phys. Rev. Lett. 91 (2003) 241804 [hep-ex/0307080].
- [52] M. Cacciari, P. Nason, JHEP 0309 (2003) 006 [hep-ph/0306212].
- [53] B.A. Kniehl, G. Kramer, I. Schienbein, H. Spiesberger, Phys. Rev. Lett. 96 (2006) 012001 [hep-ph/0508129].
- [54] N. Armesto, C.A. Salgado, U.A. Wiedemann, Phys. Rev. Lett. 94 (2005) 022002 [hep-ph/0407018].
- [55] K. Werner, hep-ph/0603064, hep-ph/0603195.
- [56] B.B. Back et al. (PHOBOS), Phys. Rev. C 65, 061901(R) (2002) [nucl-ex/0201005].
- [57] S.S. Adler et al. (PHENIX), Phys. Rev. C 71 (2005) 034908 [nucl-ex/0409015].
- [58] I.G. Bearden et al. (BRAHMS), Phys. Rev. Lett. 88 (2002) 202301 [nucl-ex/?].
- [59] G.J. Alner et al. (UA5), Z. Phys. C 33 (1986) 1.
- [60] D. Kharzeev, E. Levin, Phys. Lett. B 523 (2001) 79 [nucl-th/0108006].
- [61] S.S. Adler et al. (PHENIX), Phys. Rev. Lett 96 (2006) 012304 [nucl-ex/0507032].
- [62] G. Pauletta, J. Phys. G 31 (2005) S817.
- [63] R. Gavai, D. Kharzeev, H. Satz, G.A. Schuler, K. Sridhar, R. Vogt, Int. J. Mod. Phys. A 10 (1995) 3043 [hep-ph/0505032].
- [64] I. Abt et al. (HERA-B), Phys. Lett. B 638 (2006) 407 [hep-ex/0512029].
- [65] M. Cacciari, S. Frixione, M.L. Mangano, P. Nason, G. Ridolfi, JHEP 0407 (2004) 033 [hep-ph/0312132];
- [66] M. Cacciari, hep-ph/0407187; M.L. Mangano, hep-ph/0411020.
- [67] See, e.g., O. Nachtmann, Phänomene und Konzepte der Elementarteilchenphysik, Vieweg 1992, p. 273.
- [68] M. Glück, J.F. Owens, E. Reya, Phys. Rev. D 17 (1978) 2324.
- [69] Z. Lin, C.M. Ko, Phys. Rev. C 62 (2000) 034903 [nucl-th/9912046].
- [70] S. Datta et al., Phys. Rev. D 69 (2004) 094507.
- [71] J. Hüfner, Yu. P. Ivanov, B. Z. Kopeliovich, A. V. Tarasov, Phys. Rev. D 62 (2000) 094022.
- [72] M. E. Peskin, Nucl. Phys. B 156 (1979) 365.
- [73] J. Gosset, A. Baldisseri, H. Borel, F. Staley, Y. Terrien, Eur. Phys. J. C 13 (2000) 63 [nucl-ex/9906002].
- [74] B. Alessandro et al. (NA50), Eur. Phys. J. C 39 (2005) 335 [hep-ex/0412036].
- [75] M. Sitta et al. (NA50), J.Phys. G 30 (2004) S1175 [hep-ex/0405056].
- [76] R. Shahoyan et al. (NA60), Nucl. Phys. A 774 (2006) 677c

- [77] M.C. Abreu et al. (NA50), Nucl. Phys. A 698 (2002) 539c.
- [78] E. Schnedermann, J. Sollfrank, U. Heinz, Phys. Rev. C 48 (1993) 2462.
- [79] M.I. Gorenstein, K.A. Bugaev, M. Gaździcki, Phys. Rev. Lett. 88 (2002) 132301 [hep-ph/0112197].
- [80] M.C. Abreu et al. (NA50), Phys. Lett. B 499 (2001) 85.
- [81] J. Adams et al. (STAR), Nucl. Phys. A 757 (2005) 102 [nucl-ex/0501009]; O. Barannikova, nucl-ex/0403014.
- [82] V.N. Tram (PHENIX), nucl-ex/0606017; H. Pereira Da Costa, private communication.
- [83] S.S. Adler, et al. (PHENIX), Phys. Rev. Lett. 92 (2004) 051802 [hep-ex/0307019].
- [84] K.A. Bugaev, M. Gaździcki, M.I. Gorenstein, Phys. Lett. B 544 (2002) 127 [hep-ph/0206109].
- [85] R.L. Thews, hep-ph/0605322.